Journal of Catalysis 264 (2009) 154–162

Contents lists available at ScienceDirect

Journal of Catalysis

journal homepage: www.elsevier.com/locate/jcat

Deactivation of a $Au/CeO_2–Co_3O_4$ catalyst during CO preferential oxidation in H_2-rich stream

Hui Wang [a,b], Huaqing Zhu [a], Zhangfeng Qin [a], Feixue Liang [a,b], Guofu Wang [a], Jianguo Wang [a,*]

[a] State Key Laboratory of Coal Conversion, Institute of Coal Chemistry, Chinese Academy of Sciences, P.O. Box 165, Taiyuan, Shanxi 030001, PR China
[b] Graduate University of the Chinese Academy of Sciences, Beijing 100049, PR China

ARTICLE INFO

Article history:
Received 23 January 2009
Revised 31 March 2009
Accepted 3 April 2009
Available online 6 May 2009

Keywords:
CO preferential oxidation
CO oxidation
$Au/CeO_2–Co_3O_4$
Deactivation

ABSTRACT

The origins of the deactivation of a $Au/CeO_2–Co_3O_4$ catalyst during CO preferential oxidation (PROX) are investigated in detail by means of high-resolution transmission electron microscopy (HRTEM), X-ray diffraction (XRD), X-ray photoelectron spectroscopy (XPS), temperature-programmed reduction of hydrogen (H_2-TPR), temperature-programmed oxidation of oxygen (O_2-TPO), and diffuse reflectance infrared Fourier transform spectroscopy (DRIFTS). A possible mechanism involving –OOH intermediate is proposed and used to explain the deactivation in the long-term stability test of CO PROX. The aggregation or sintering of the Au particles is excluded from the origins of deactivation by HRTEM and XRD. The deactivation of the catalyst is mainly due to an intrinsic transformation in the chemical state of the gold species and the support oxides in the $Au/CeO_2–Co_3O_4$ catalyst. The XPS, XRD, and H_2-TPR results demonstrate the reduction of ionic Au to metallic Au and of cobalt oxide to cobaltous compound. The changes of the chemical states imply a structure reordering of the catalyst surface, which will suppress the supplement of active oxygen and the formation of –OOH species, inhibit the CO oxidation reaction, and lead to the deactivation of the catalyst. The accumulation of carbonates and H_2O on the deactivated catalyst is revealed by XPS, DRIFTS, O_2-TPO, and a regeneration test. They are responsible for the complete deactivation of the catalyst. The hydration of the catalyst surface may play a more important role than the formation of carbonates in the deactivation of the catalyst.

1. Introduction

Polymer electrolyte membrane fuel cells (PEMFCs) have attracted much attention as a potential power source of electric vehicles due to their low operation temperature, excellent energy efficiency, and zero-emission of air pollutants. Hydrogen is the preferred fuel for PEMFCs. However, there are still many problems related to the issue of hydrogen distribution and storage. On board reforming of liquid fuels followed by water-gas shift (WGS) reaction is one of the alternatives to produce hydrogen for fuel cells. In addition to hydrogen, the resulting reformer gas still contains a trace amount of CO, which has a devastating effect on the energy conversion efficiency of the fuel cells via CO-induced poisoning of the Pt anode catalyst [1].

Among the current available methods, CO preferential oxidation (PROX) seems to be the most economic and straightforward one to reduce the CO contamination to the parts per million level. Catalysts so far proposed for this process are mainly the platinum group metal (Pt, Ru, and Rh) catalysts [2–4], Cu-based catalysts [5], and gold-based catalysts [6]. The platinum group metal catalysts have desirable activity and stability at a temperature in the range of 150–200 °C, but they are not selective enough in the presence of H_2O and CO_2, and their high cost may limit their applicability for transportation applications [7]. The performance of $CuO–CeO_2$ mixed oxide catalysts is superior to that of Pt group-based catalysts, since they are more active and remarkably more selective at a lower reaction temperature [8]. Gold-based catalysts have recently been proposed as promising candidates for the selective removal of CO from reformate streams [1,6,9–12]. They are found to be more active than the platinum group metal catalysts and Cu-based catalysts at relatively low temperatures. Extensive efforts have been put into the preparation, characterization, and testing of gold catalysts, however, as commented by Bond and Thompson, one of the unsatisfactory aspects of gold catalysis research is that the possible changes in the conversion with time on stream are typically not reported or only qualitatively mentioned [13,14]. As the commercial application of gold catalysts is being pursued, it is essential to understand the mechanism for the reaction and deactivation [15].

As for the mechanism concerned, the most representative model was proposed by Bond and Thompson in 2000 [16]. Au atoms at the interface between the Au particle and the oxide are the active oxidation centers. However, it is unclear whether cationic Au or

* Corresponding author. Fax: +86 351 4041153.
E-mail address: iccjgw@sxicc.ac.cn (J. Wang).

0021-9517/$ - see front matter © 2009 Elsevier Inc. All rights reserved.
doi:10.1016/j.jcat.2009.04.003

metallic Au is the active site of gold [17,18]. Steyn et al. reported that the reduction of ionic Au is responsible for CO PROX over Au/TiO_2 [19]. Haruta [20] has reassessed the mechanism of CO oxidation developed by Bond and Thompson. It is suggested that CO is activated by adsorption onto Au^0 on the surface of the gold nanoparticles, and that O_2 is activated by the atoms at the boundary between the support and the gold nanocrystals. The atoms at the boundary are proposed to be oxidic Au species in nature. As for the deactivation of the gold catalyst, the accumulation of carbonate species and growth in the size of the gold particles are the generally accepted mechanisms [21]. It is suggested that the severe deactivation might result from the sintering of the Au nanoparticles under a hydrogen atmosphere, but several studies have shown that hydrogen treatment of gold catalyst favors the formation of smaller Au particles [22,23]. It has been suggested that the carbonate and water formed on the oxygen-deficient sites cause the deactivation of the gold-based catalysts [24]. Burch suggested that a high concentration of CO_2 inhibits the activation of O_2 and causes a destruction of the intimate contact between the gold particles and the support, and that the role of water is to accelerate the destruction of the interaction between the Au particles and the support [25]. In addition, the performance and deactivation of the gold catalyst have also been linked to the characteristics of the reducible oxide supports [26]. Up to date an exact mechanism for gold-based catalysts has not been fully revealed.

Recently, we reported the preparation and catalytic activity tests of $Au/CeO_2–Co_3O_4$ with different Ce/Co atomic ratios for CO PROX in a H_2-rich stream [27]. The catalyst $Au/CeO_2–Co_3O_4$ with Ce/Co atomic ratio being 0.2 exhibits much higher stability; the stability test lasts for about 306 h with the CO conversion being between 94% and 15% and PROX selectivity being between 52% and 35%.

The objective of this work is to gain some information on the chemical and physical origins in the deactivation of the $Au/CeO_2–Co_3O_4$ catalyst. Therefore, after the long-term life test of CO PROX the deactivated $Au/CeO_2–Co_3O_4$ (Ce/Co = 0.2) catalyst is characterized in detail by means of high-resolution transmission electron microscopy (HRTEM), X-ray diffraction (XRD), X-ray photoelectron spectroscopy (XPS), temperature-programmed reduction of hydrogen (H_2-TPR), temperature-programmed oxidation of oxygen (O_2-TPO), and diffuse reflectance infrared Fourier transform spectroscopy (DRIFTS) of CO adsorption. Based on the investigation, the possible mechanism for the PROX reaction of CO on $Au/CeO_2–Co_3O_4$ is proposed and employed to explain the deactivation process of the catalyst.

2. Experimental

2.1. Catalyst preparation

$CeO_2–Co_3O_4$ composite oxide was prepared by sol-gel precipitation as described elsewhere [27,28]. Briefly, the alcosol was obtained through the hydrolysis of $Co(NO_3)_2 \cdot 6H_2O$ and $Ce(NO_3)_3 \cdot 6H_2O$ in ethanol under stirring. The precipitation was achieved with sodium hydroxide solution at an ambient temperature. After aging, washing, and exchanging water with ethanol, the wet precipitate was dried at 120 °C and was finally calcined at 500 °C in air for 3 h. Au-supported catalyst was prepared through deposition-precipitation method. $HAuCl_4$ and NaOH aqueous solutions were added dropwise into the suspension of $CeO_2–Co_3O_4$ composite oxide under vigorous stirring with a constant pH value of 8.0 at a temperature of 70 °C. After aging and filtration, the precipitate was washed several times with deionized water till no chlorine ions were detected by $AgNO_3$ solution. The resulting material was then dried at 120 °C for 12 h and was calcined at 200 °C for 2 h. The Ce/Co atomic ratio was 0.2 for the $CeO_2–Co_3O_4$ composite oxide and the Au loading was 1 wt.% for the Au-supported catalyst. The composition of the catalyst was measured by inductively coupled plasma-atomic emission spectrometry (ICP-AES).

2.2. Catalytic tests and analytical procedure

The catalytic test for CO PROX in a hydrogen-rich stream was carried out in a quartz tubular flow microreactor with an internal diameter of 6.0 mm at atmospheric pressure as described previously [27,28]. The catalyst was evaluated in the fresh state without any pretreatment. The reacting stream consisted of 1.0% CO + 1.0% O_2 + 50.0% H_2 (by volume), balanced with Ar, and the space velocity was 30,000 ml g^{-1} h^{-1}. CO and CO_2 in the effluent gas were periodically analyzed online with a gas chromatograph equipped with a column packed with carbon molecular sieve, a post-column methanator that converted CO and CO_2 into CH_4, and a flame ionization detector (FID). The consumption of oxygen was also periodically determined online with a gas chromatograph equipped with a column packed with 13X molecule sieve and a thermal conductivity detector (TCD). The activity was then evaluated on the basis of CO and O_2 conversion, which can be calculated with the CO and O_2 concentrations in the reactant gas and in the effluent gas. The selectivity of CO PROX was defined as the fraction of O_2 consumption for the CO oxidation to CO_2 over the total O_2 consumption.

2.3. Catalyst characterization

XRD was performed on an advanced X-ray diffractometer (Bruker AXS D8, Germany). The diffraction patterns of the samples were recorded at room temperature with Cu Kα radiation in the range of 2θ between 10° and 85°. The average crystallite size was estimated from the line broadening of the most intense XRD reflections with Scherrer formula [27,28].

The HRTEM images of the samples were obtained using a JEM 2010 microscope operating at 200 kV and equipped with an energy-dispersive X-ray (EDX) instrument. The catalyst was crushed to a fine powder, and then a holey carbon film copper grid was dipped into the crushed powder.

H_2-TPR was performed in a quartz microreactor, and about 50 mg sample was used in each measurement as described elsewhere [27,28]. The fresh catalyst was first pretreated under an air flow at 200 °C for 1 h, and was then purged with Ar at the same temperature for 1 h and cooled to room temperature. The flow of 5% H_2 in Ar (30 ml/min) was then switched into the system, and the sample was heated up to 500 °C from room temperature at a rate of 10 °C/min. For the deactivated sample, the same procedure was carried out except the pretreatment. The amount of H_2 uptake during the reduction was measured by TCD, which was calibrated by the quantitative reduction of CuO to the metallic copper.

XPS was performed on a VG MiltiLab 2000 spectrometer with Mg Kα radiation and a multichannel detector. Approximately 100 mg of the sample powder was compressed into a wafer for analysis. The survey spectra were measured in the range of 0–1100 eV binding energy (BE), and detail spectra of the Au 4f, Ce 3d, and Co 2p regions were measured in the ranges 80–90 eV, 875–925 eV, and 775–810 eV, respectively. The BEs were calibrated using the C 1s signal located at 284.6 eV.

O_2-TPO was performed in a quartz microreactor, and about 50 mg sample was used in each measurement. The samples were purged in an Ar flow at 200 °C for 1 h and were cooled to room temperature prior to the analysis. The flow of 6% O_2 in Ar (30 ml/min) was then switched into the system, and the sample was heated up to 500 °C from room temperature at a rate of 10 °C/min. The amounts of O_2, CO, CO_2, H_2, and H_2O in the outlet gas

were measured with a mass spectrometer OmniStar equipped with the software Quadstar 32-bit. The intensity of CO and H_2 signals was calibrated using CO(5%)/Ar and H_2(5%)/Ar, respectively. CO_2 signal was calibrated by the pulse of pure CO_2 with a six-port pulsing valve.

DRIFTS was carried out on a Nicolet 380 FT-IR spectrometer equipped with a MCT/A detector at a spectral resolution of 4 cm^{-1} (accumulating 32 scans). Prior to the measurement, the sample was treated in situ at 200 °C in 5% O_2/Ar (30 ml min^{-1}) to eliminate possible water traces. After cooling to room temperature in a flow of pure argon, a background spectrum was collected for spectra correction. Then, a flow of 3% CO or 1% CO + 50% H_2 with or without 1% O_2 in Ar was introduced into the DRIFTS chamber, and the spectra of CO adsorption on the catalyst samples were collected.

3. Results and discussion

3.1. Long-term stability test

The long-term stability test on Au/CeO_2–Co_3O_4 catalyst for CO PROX in a hydrogen-rich stream was carried out at 80 °C, as shown in Fig. 1. During the first 100 h of time on stream (TOS), the CO conversion and CO_2 selectivity decreased drastically from 94% to 71% and 52% to 37%, respectively, and then leveled off in the following 160 h. The O_2 conversion did not change observably during the first 260 h of TOS. However, in the subsequent 40 h, the decrease in both O_2 and CO conversion speeded up. The catalyst lost its activity at various rates in the different periods of TOS, which may imply that the origins of the deactivation are different in the corresponding periods of the CO PROX process. Therefore, the used catalyst was then characterized in detail in comparison with the fresh catalyst. The possible changes in the physical and chemical properties of the catalyst during the reaction process were studied, and then an explanation for the observation in the stability test was proposed.

3.2. XRD

XRD patterns of the fresh and deactivated Au/CeO_2–Co_3O_4 catalysts are shown in Fig. 2. Ceria fluorite and Co_3O_4 spinel phases are present in the fresh catalyst. The crystal sizes of CeO_2 from fluorite (1 1 1) plane and Co_3O_4 from spinel (3 1 1) plane are 3 nm and 13.1 nm, respectively. These two phases are also present in the deactivated catalyst, but their diffraction intensity decreases significantly, indicating that such crystals in the bulk may transfer to amorphous phase. Meanwhile, a new phase ascribed to CoO is observed in the deactivated catalyst, indicating a phase transformation from Co_3O_4 to CoO. The transformation of the phases reveals that the chemical state of the support oxides changes, and that the catalyst surface restructure is present during the long-term stability test. No diffraction peaks of gold species are detected in any catalyst samples.

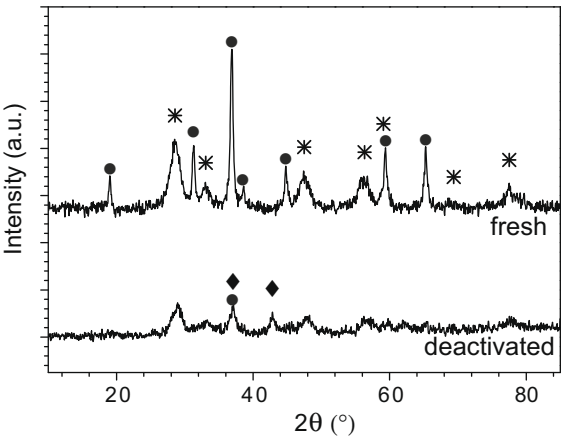

Fig. 2. XRD patterns of the fresh and deactivated Au/CeO_2–Co_3O_4 catalysts. Crystalline phases detected: ∗ CeO_2; • Co_3O_4; ◆ CoO.

3.3. HRTEM

The HRTEM images of the fresh and deactivated Au/CeO_2–Co_3O_4 catalysts are shown in Fig. 3. The reflection with a d spacing value of 0.31 nm corresponding to CeO_2 (1 1 1) plane and the CeO_2 (2 0 0) reflection with a spacing value of 0.27 nm are observed in the fresh sample. In the deactivated catalyst, besides the lattice plane (1 1 1) and (2 2 0) of fluorite CeO_2, the reflection of CoO (1 1 1) with a spacing value of 0.26 nm is detected. However, no reflections related to gold species are detected either in the fresh catalyst or in the deactivated catalyst although the presence of Au in the samples has been confirmed by the EDX spectroscopy and ICP-AES analysis. Combined with the XRD result, the observation indicates that neither aggregation nor sintering of the gold particles occurs during the long-term CO PROX reaction process.

3.4. H_2-TPR

The H_2-TPR profiles of the fresh and deactivated Au/CeO_2–Co_3O_4 catalysts are shown in Fig. 4, and the quantitative result is listed out in Table 1.

In the fresh catalyst, the following reaction may be involved in the H_2-TPR process:

$$Au_2O + H_2 \rightarrow 2Au + H_2O \quad (1)$$

$$2CeO_2 + H_2 \rightarrow Ce_2O_3 + H_2O \quad (2)$$

$$Co_3O_4 + H_2 \rightarrow 3CoO + H_2O \quad (3)$$

$$CoO + H_2 \rightarrow Co + H_2O \quad (4)$$

The consumption of H_2 below 100 °C is attributed to the reduction of surface oxygen species and Au species in high valence (Eq. (1)) as discussed in the previous work [27]. Above 100 °C, two reduction peaks at 175 °C (α) and ca. 350 °C (β) are detected for the fresh catalyst. With respect to H_2-TPR of Au/CeO_2 catalyst [27], the peak α should be attributed to the reduction of Ce^{4+} to Ce^{3+} (Eq. (2)). However, as listed out in Table 1, the H_2 consumption of peak α is

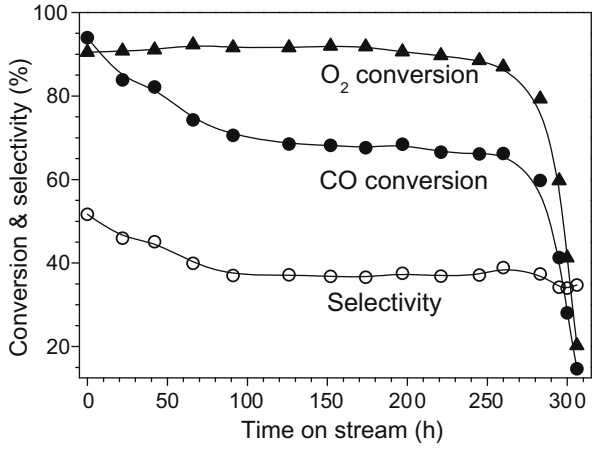

Fig. 1. Long-term stability test for CO PROX on the Au/CeO_2–Co_3O_4 catalyst at 80 °C. Reaction gas: 1.0% CO, 1.0% O_2, 50.0% H_2, balanced with Ar; space velocity, 30,000 ml g^{-1} h^{-1}.

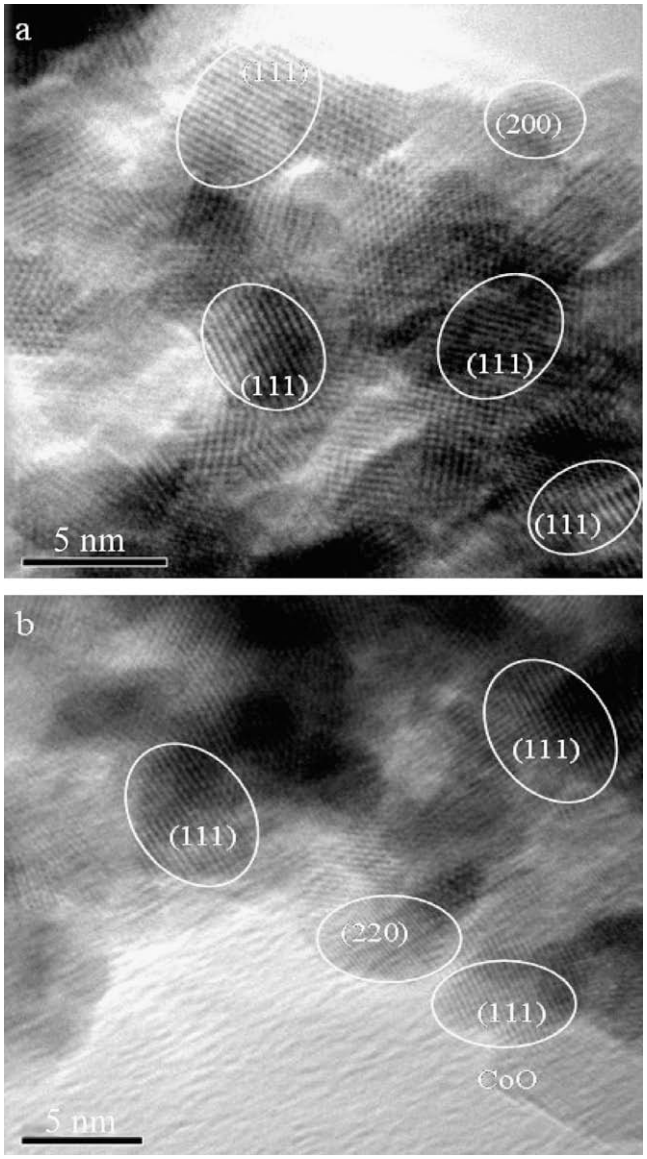

Fig. 3. High-resolution transmission electron microscopic images of the fresh (a) and deactivated (b) $Au/CeO_2–Co_3O_4$ catalysts.

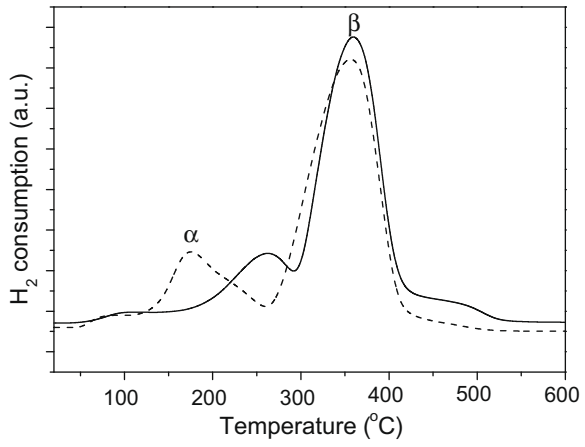

Fig. 4. H_2-TPR profiles of the fresh (---) and deactivated (—) $Au/CeO_2–Co_3O_4$ catalysts.

Table 1
H_2-TPR results for the fresh and deactivated $Au/CeO_2–Co_3O_4$ catalysts.

Catalyst[a]	H_2 uptake (μmol/g)		Reducible Co_3O_4[b] (μmol/g)	Reducible CoO[c] (μmol/g)	Reducing degree[d] (%)
	Peak α	Peak β			
Fresh	2110	7872	1247	4131	91
Deactivated	1585	7091	722	4925	82

[a] The atomic ratio of Ce/Co is 0.2, corresponding to CeO_2 content of 1726 μmol/g and cobalt atom content of 8627 μmol/g in the $Au/CeO_2–Co_3O_4$.

[b] Reducible Co_3O_4 (R_1) is calculated from the H_2 uptake of peak α ($H\alpha$) with the deduction of the H_2 uptake (863 μmol/g) due to the reduction of CeO_2: $R_1 = H\alpha - 863$.

[c] Reducible CoO (R_2) is calculated from the H_2 uptake of peak β (H_β) with the deduction of the H_2 uptake due to the stepwise reduction of CoO to Co that originated from the reduction of Co_3O_4: $R_2 = H_\beta - 3R_1$.

[d] Reducing degree is determined as the proportion of Reducible Co_3O_4 and CoO ($R_1 + R_2$) to the stoichiometric number of cobalt atoms (N = 8627 μmol/g) in the catalyst.

2110 μmol/g, which is much higher than the amount of hydrogen required for the stoichiometric reduction of CeO_2 to Ce_2O_3 (863 μmol/g), so the extra hydrogen consumption (1247 μmol/g) should be ascribed to the simultaneous reduction of Co_3O_4 to Co^{2+} (Eq. (3)). The peak β is ascribed to the reduction of Co^{2+} to Co^0 (Eq. (4)) [27,29]. The corresponding hydrogen consumption is 7872 μmol/g. After deduction of the H_2 uptake for the subsequent reduction of CoO from Co_3O_4 (Eq. (3)), the hydrogen consumption for the original CoO in the fresh catalyst is about 4131 μmol/g. In other words, 1247 μmol/g of Co_3O_4 and an extra 4131 μmol/g of CoO in the fresh catalyst are reduced to Co^0 in the whole H_2-TPR process. The stoichiometric number of cobalt atoms (N) is 8627 μmol/g in the $Au/CeO_2–Co_3O_4$ catalyst with the Ce/Co atomic ratio of 0.2, so the proportion of reduced cobalt to N is about 91%.

For the deactivated catalyst, the temperature of the peak α is 110 °C higher than that for the fresh $Au/CeO_2–Co_3O_4$ catalyst, indicating that the reduction of ceria and cobalt oxide becomes difficult in the deactivated catalyst due to the change in the interaction between ceria and cobalt oxide. The position of peak β does not change obviously. However, a small broad peak at 472 °C becomes observable, which is ascribed to the reduction of CoO interacting with ceria [29]. From the quantitative result as listed out in Table 1, it can be seen that the H_2 consumption of both peak α and peak β decreases. The reduced Co_3O_4 and an extra CoO are of 722 and 4925 μmol/g, respectively, in the deactivated catalyst. The proportion of reduced cobalt ions is about 82%, which is less than that in the fresh catalyst, indicating that the reduction of cobalt oxide becomes difficult in the deactivated catalyst. Although the reducible cobalt ions decrease, the amount of CoO reduced increases. This result suggests that more CoO is present in the deactivated catalyst than in the fresh catalyst, which is consistent with the HRTEM and XRD results.

3.5. XPS

To examine the chemical species on the fresh and deactivated catalysts, XPS measurement was performed.

The XPS spectra in the Au 4f region of the fresh and deactivated catalysts are shown in Fig. 5. Deconvolution of the Au spectra indicates that both metallic and ionic gold species are present in the fresh catalyst. The first doublet with peaks at 84.0 and 87.7 eV is the characteristic of Au^0, and the peaks at 84.9 and 88.6 eV are assigned to $Au^{\delta+}$ [30]. However, only metallic gold is observed in the deactivated catalyst. Since $Au^{\delta+}$ is considered to be the more active species than Au^0 for CO oxidation, the reduction of $Au^{\delta+}$ is one of the reasons for the deactivation. The surface concentrations of gold

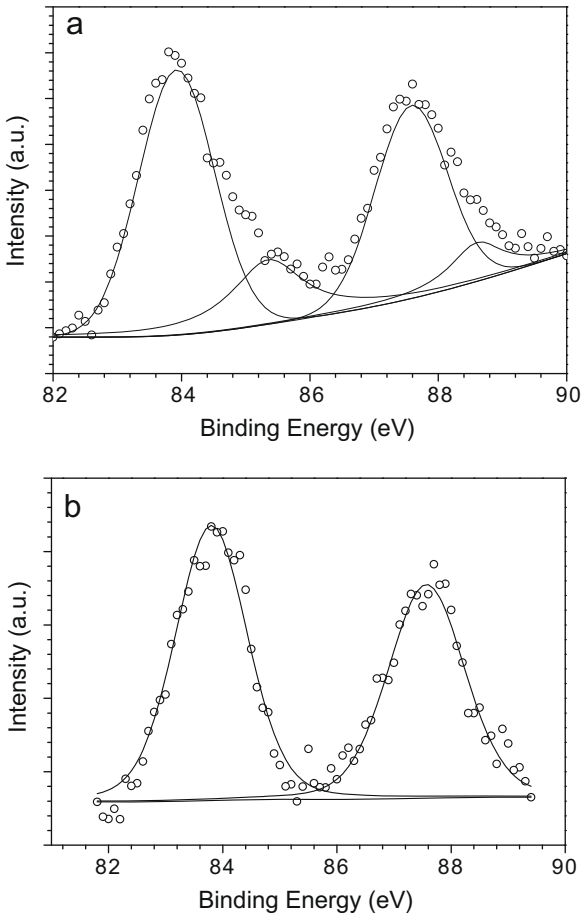

Fig. 5. X-ray photoelectron spectra in the Au 4f region for the fresh (a) and deactivated (b) $Au/CeO_2–Co_3O_4$ catalysts.

measured by XPS are about 0.43 at.% (the atomic ratio of Au to the total metal atoms) and 0.35 at.% on the fresh and deactivated catalysts. Both of them are lower than the bulk gold content (0.48 at.%). The group of Flytzani-Stephanopoulos [12,31] also found that the surface gold content of Au/CeO_2 decreases after PROX reaction. They suggested that only strongly bound gold in ceria appears to be involved in catalyzing the PROX reaction. Therefore, it is deduced that the disappearance of $Au^{\delta+}$ may indicate the destruction of the strong interaction between gold and ceria and a decrease in the amount of strongly bound gold to ceria in the deactivated catalyst.

Fig. 6a shows the XPS spectra in the Ce 3d region. The four main $3d_{5/2}$ features at 882.7, 885.2, 888.5, and 898.3 eV correspond to V, V′, V″, and V‴ components, while the $3d_{3/2}$ features at 901.3, 903.4, 907.3, and 916.9 eV correspond to U, U′, U″, and U‴ components, respectively [32]. The signals V′ and U′, characteristics of Ce^{3+}, exist in the fresh catalyst [33], but they are not so evident for the deactivated catalyst. The presence of Ce^{3+} is contributed to the interaction between ceria and the surrounding atoms. Kang et. al [34] reported that the interaction between ceria and cobalt oxide may lead to a transfer of the lattice oxygen in ceria into the lattice of cobalt oxide and retain cobalt at the high-valent state. It was also reported that the gold at the perimeter of the gold nanoparticles with the ceria or the ultrasmall Au clusters located near an oxygen vacancy may bear a positive charge [35]. Liu et. al [36] investigated the most likely binding site of Au on ceria. They found that Au atoms can be oxidized by the surface Ce atoms ($Au \rightarrow Au^{\delta+}$ and $Ce^{4+} \rightarrow Ce^{3+}$) even though there is no direct Ce–Au bonding. This is the reason for the presence of $Au^{\delta+}$ and Ce^{3+} in the fresh $Au/CeO_2–Co_3O_4$ catalyst. Combined with the H_2-TPR result, it is deduced that Au prefers to interact with ceria with respect to cobalt [27]. In summary, the decrease of Ce^{3+} and $Au^{\delta+}$ in the deactivated catalyst indicates the weakness of the interactions both between ceria and gold and between ceria and cobalt oxide.

Fig. 6b shows the XPS spectra in the Co 2p region. It is difficult to distinguish Co^{2+} from Co^{3+} by Co 2p spectra due to the small difference in their BE values. The spin–orbit splitting of the Co 2p peaks (ΔE) is found to be well correlated with the oxidation state of cobalt [37]. The value of ΔE is 16.0 eV for CoO [38], 15.0 eV for the cobaltic compounds (Co_2O_3), and 15.2 eV for the mixed-valence Co_3O_4 [37]. The ΔE values of Co 2p features in the fresh and deactivated $Au/CeO_2–Co_3O_4$ catalysts are listed out in Table 2. The ΔE value of 15.2 eV is detected for the fresh catalyst, so Co_3O_4 is the main phase in the fresh sample. In the deactivated catalyst, however, the value of ΔE is observed to be 15.5 eV, indicating an increase of CoO phase in the material. This result is in good agreement with that of XRD and HRTEM. The increase of the cobalt oxide in low valence means a weakness of the interaction between cobalt oxides and ceria, which leads to a decrease of the oxygen vacancies [39].

The Ce/Co atomic ratios on the catalyst surface determined by XPS are listed out in Table 2 as well. It is noticed that the surface Ce/Co atomic ratios, 0.44 for the fresh catalyst and 0.35 for the deactivated one, are remarkably higher than the nominal value (0.2) in the catalyst bulk. The increase of the ratios suggests that the surface is cerium-rich, which is consistent with the result of HRTEM. Compared with the fresh catalyst, the surface Ce/Co of the deactivated catalyst decreases, indicating that the cerium-rich oxide structure is reordered [40].

The XPS spectra of O 1s shown in Fig. 6c show two BE peaks for both the fresh and deactivated catalysts. The lower BE band at 529-530 eV corresponds to O^{2-} anions of cerium oxide and cobalt oxide, and the higher BE band at ca. 531 eV corresponds to O^{2-} of the surface carbonates and hydroxides of cerium and cobalt [40]. For the deactivated catalyst, the O^{2-} peak tends to shift toward higher BE value than for the fresh catalyst. Combined with the observation that the surface Ce/Co atomic ratio decreases in the deactivated catalyst, it can be deduced that the low contribution of the oxygen from CeO_2 to the catalyst surface leads to the increase of the O 1s BE.

The C 1s spectra shown in Fig. 6d indicate the presence of two different carbon species on the catalyst surface: adventitious carbon (284.6 eV), and formate or carbonate (288.4 eV) [24]. The surface carbonate-like species increases on the deactivated catalyst than on the fresh catalyst, which can be taken as the evidence that carbonate-like species form during the CO PROX reaction process on the $Au/CeO_2–Co_3O_4$ catalyst.

In summary, the result of XPS demonstrates that the chemical species on $Au/CeO_2–Co_3O_4$ catalyst endure changes after the long-term reaction of CO PROX. The ionic Au and cobalt oxide are reduced to metallic gold and CoO, respectively. To some extent, the surface cerium-rich oxide structure is destroyed, and the accumulation of the surface carbonate-like species is also observed. The chemical or structural reordering may be responsible for the deactivation of $Au/CeO_2–Co_3O_4$ catalyst.

3.6. O_2-TPO

As described above, the XPS reveals the increase of the carbonate-like species on the deactivated $Au/CeO_2–Co_3O_4$ catalyst. For many catalysts, carbonaceous species accumulation can be removed, at least partially, via calcination in air or O_2, so O_2-TPO is performed to determine the possible presence of the carbonaceous species on the $Au/CeO_2–Co_3O_4$ catalysts.

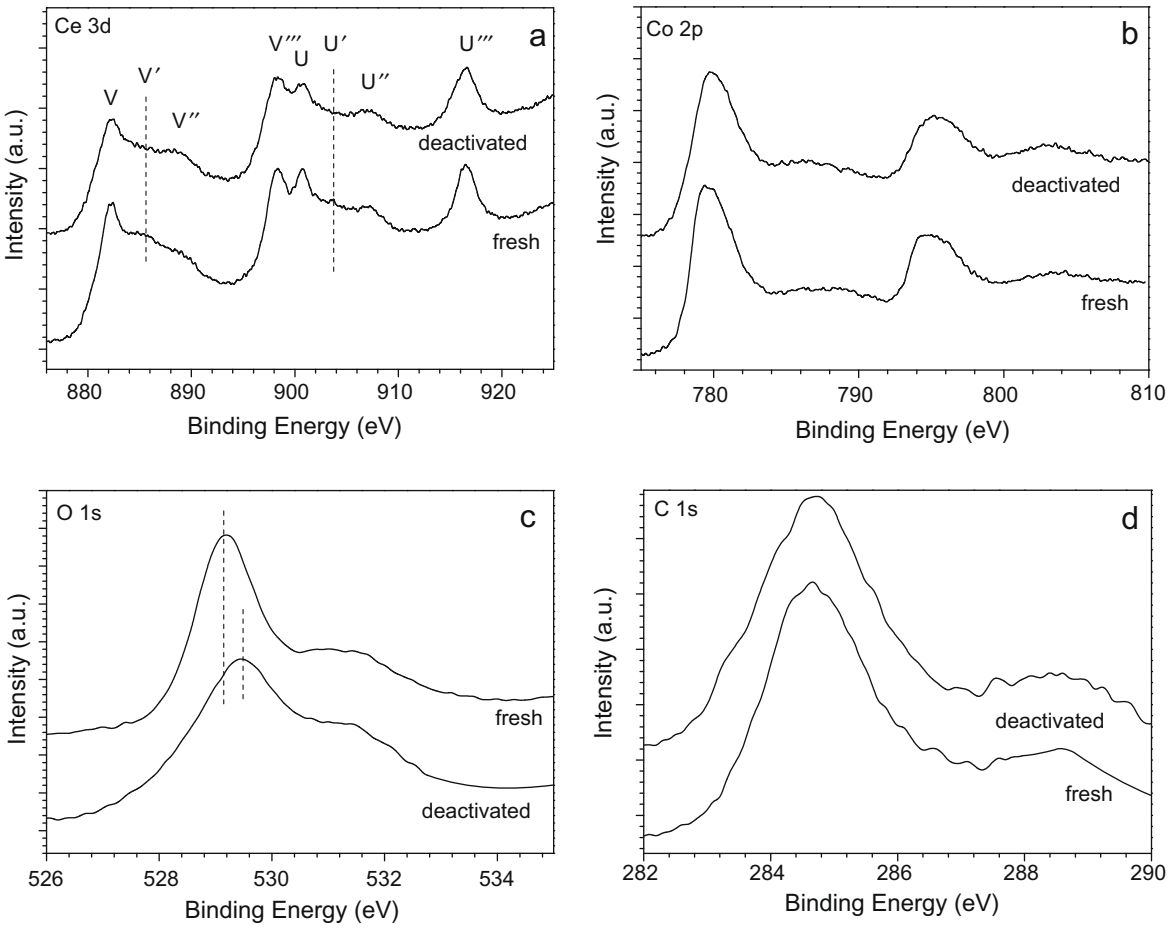

Fig. 6. X-ray photoelectron spectra in the Ce 3d (a), Co 2p (b), O 1s (c), and C 1s (d) regions for the fresh and deactivated $Au/CeO_2–Co_3O_4$ catalysts.

The mass spectra of O_2, CO_2, and H_2O in O_2-TPO processes on the deactivated $Au/CeO_2–Co_3O_4$ catalyst are illustrated in Fig. 7. No CO_2 is detected for the fresh catalyst (not shown), while large amounts of CO_2 and H_2O are produced on the deactivated catalyst at temperatures between 150 and 250 °C accompanied with the consumption of oxygen. The oxidation of surface carbon is reported at about 450 °C [41], so the production of CO_2 and H_2O at such a low temperature is probably due to the decomposition of carbonate-like species. The consumption of oxygen calculated from the mass signal of O_2 is about 1926 μmol/g, which is ascribed to the oxidation of Co^{2+}. The results demonstrate the formation of carbonate-like species and a reduction of the support oxides during the CO PROX reaction process on the $Au/CeO_2–Co_3O_4$ catalyst.

3.7. DRIFTS of CO adsorption in different atmospheres on the $Au/CeO_2–Co_3O_4$ catalyst

In order to gain some insights into the CO PROX reaction mechanism and the role of the mixed oxides support, *in situ* DRIFTS of CO adsorption in different atmospheres was performed. For all the samples, the bands in the region of 2300–2400 $cm^{-1}$are assigned to gaseous CO_2, the bands in the region of 2050–2200 $cm^{-1}$are ascribed to CO-related species [37], and the weak peaks at 1050 and 1120 cm^{-1} are attributed to carbonates [42].

3.7.1. CO adsorption

Fig. 8a shows the spectra of CO adsorption on the $Au/CeO_2–Co_3O_4$ catalyst in the CO/Ar flow at room temperature, namely

Table 2
XPS results for the fresh and deactivated $Au/CeO_2–Co_3O_4$ catalysts: binding energy of Co 2p and atomic ratio of Ce/Co on the sample surface.

Catalyst	Binding energy (eV)				Ce/Co
	Co $2p_{3/2}$	Co $2p_{1/2}$	ΔE	Ce $3d_{5/2}$	
Fresh	779.4	794.6	15.2	882.4	0.44
Deactivated	779.8	795.3	15.5	882.3	0.35

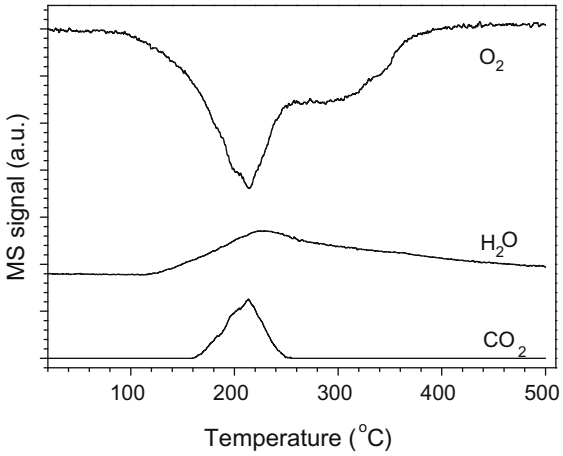

Fig. 7. Mass spectra of CO_2, H_2O, and O_2 during O_2-TPO on the deactivated $Au/CeO_2–Co_3O_4$ catalyst.

20 °C. In the carbonyl region (2000–2200 cm^{-1}), the bands at 2170 and 2120 cm^{-1} are ascribed to the absorption of CO gas. No carbonyl species related to Au are detectable in the measurement, which may be due to the Au carbonyl species that are so active at ambient temperature: as soon as they are produced, they react with the lattice oxygen of the catalyst to form CO_2. In fact, the CO adsorption on supported Au is generally measured at a very low temperature such as −183 °C [43].

Upon CO admission, two strong bands ascribed to gaseous CO_2 are observed at 2359 and 2340 cm^{-1}, suggesting that the CO oxidation has taken place over the catalyst even at an ambient temperature. In the first 3 min, the intensity of CO_2 increases with the adsorption time, but then it decreases gradually and almost disappears finally. Upon heating, as shown in Fig. 8b, the intensity of CO_2 increases with an increase in the temperature. Combined with the H_2-TPR result, the formation of CO_2 at a temperature below 100 °C may originate from the reaction between the adsorbed CO and the surface adsorbed oxygen species, while it can be mainly ascribed to the participation of lattice oxygen of CeO_2 and Co_3O_4 oxides in the CO oxidation reaction at a temperature above 100 °C.

The result suggests that the role of the CeO_2–Co_3O_4 composite oxide in CO oxidation is not only in providing active centers for the oxygen activation but also in releasing-uptaking oxygen through redox processes realized by Ce^{4+}/Ce^{3+} and Co^{3+}/Co^{2+} couples. At room temperature, the CO molecules adsorbed on gold sites react with the surface oxygen species to form CO_2. After the readily surface oxygen species are depleted, the CO oxidation rate decreases. Upon heating, the bulk lattice oxygen migrates to the surface of the oxides and reacts with the adsorbed CO molecules to form CO_2 again [44].

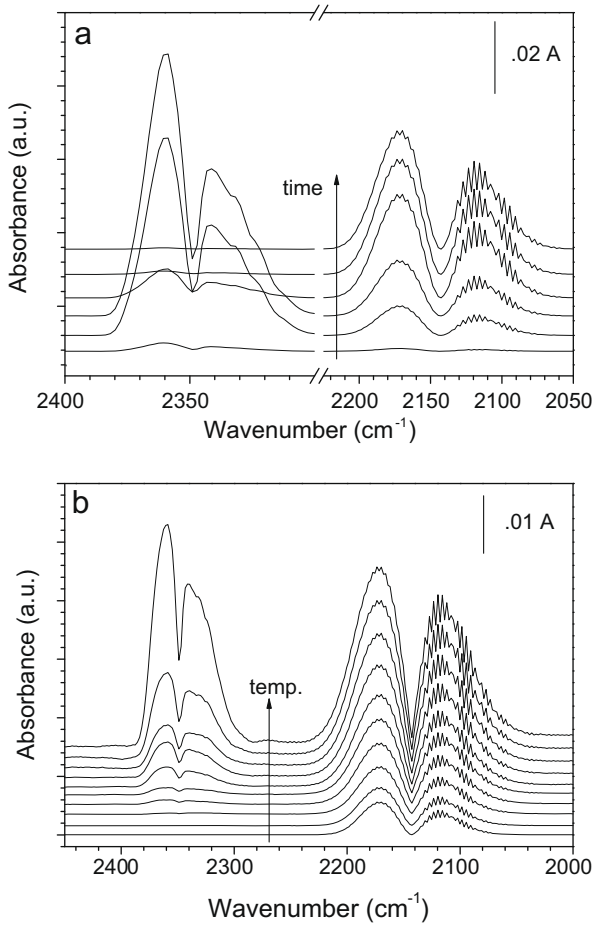

Fig. 8. DRIFTS spectra of CO adsorption in the 3% CO/Ar flow on the Au/CeO_2–Co_3O_4 catalyst. (a) At room temperature (20 °C) with the adsorption time of 1, 2, 3, 4, 6, and 8 min; (b) at different temperatures of 20, 40, 60, 80, 100, 120, 140, 160, 180, and 200 °C.

3.7.2. CO/H_2 co-adsorption

CO/H_2 co-adsorption on the Au/CeO_2–Co_3O_4 catalyst at different temperatures is shown in Fig. 9. Upon CO/H_2 admission, the bands corresponding to CO_2 appear at room temperature. Compared with the DRIFTS spectra of CO adsorption shown in Fig. 8, the presence of H_2 enhances the CO oxidation at a temperature below 80 °C, which means that the presence of H_2 may accelerate the surface lattice oxygen mobility to some extent. However, it is noticed that the CO oxidation rate shows no difference at a temperature above 80 °C. Under the condition without oxygen, hydrogen might react with the lattice oxygen of the oxides to form H_2O and/or −OH group. The positive effect of H_2 for CO oxidation at near ambient temperature has been reported before [45]. It is suggested that such an effect is attributed to the formation of the surface hydroxyls species adjacent to the gold in the presence of H_2, which can react with the adsorbed CO to produce CO_2 [46]. However, the adsorption of the surface hydroxyls may suppress the adsorption of CO and inhibit the reaction between CO and hydroxyl [47]. Thus, the formation of the surface hydroxyls leads to both the positive effect via the supplementary pathway for CO oxidation and the negative effect via the competitive adsorption with CO on the same sites. Thus, the stable rate of CO oxidation at above 80 °C may be the result of the balance between the positive and the negative effects of the surface hydroxyls.

The very weak peaks at 1050 and 1120 cm^{-1} observed above 100 °C are ascribed to the surface carbonate species over CoO [42]. Such species are formed through the reaction of CO with the lattice oxygen of Co_3O_4. Since no oxygen is present in the gas stream to oxidize the reduced centers, the produced CO_2 can adsorb onto the centers to form surface carbonate.

3.7.3. $CO/H_2/O_2$ co-adsorption

Fig. 10 shows the $CO/H_2/O_2$ co-adsorption at different temperatures on the Au/CeO_2–Co_3O_4 catalyst. It is noticed that the intensity of CO_2 increases with an increase in the temperature. Obviously, the addition of oxygen improves the CO oxidation rate. The intense band located at ∼1620 cm^{-1} is ascribed to the δ(HOH) vibration mode of adsorbed water. A large band develops quickly in the 3500–3200 cm^{-1} region, which is related to the ν(O-H) vibration mode in hydrogen-bonded hydroxyl groups and water adsorbed on the catalyst surface [48]. As a matter of fact, Quinet et al. have

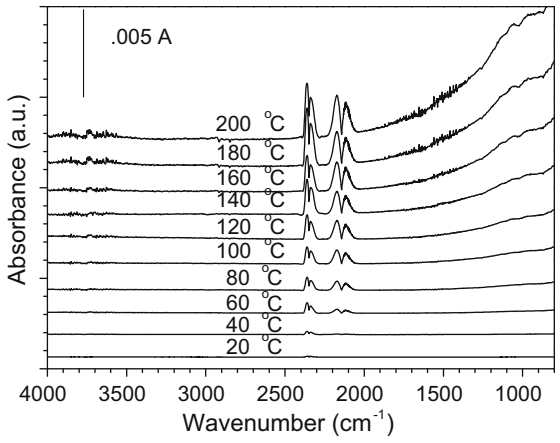

Fig. 9. DRIFTS spectra of CO/H_2 co-adsorption in (1% CO + 50% H_2)/Ar flow on the Au/CeO_2–Co_3O_4 catalyst at different temperatures.

recently detected a DRIFTS band centered at ~3250 cm^{-1} on unsupported gold under PROX conditions [49]. Piccolo et al. proposed that the bands at ~3250 cm^{-1} are related to OH (or OOH) species loosely bonded on the Au particles and/or at their periphery [48]. A recent kinetic study shows that the direct synthesis of water over silica-supported gold nanoparticles relies on the formation of hydrogen peroxy surface species (–OOH) from the reaction between the associatively adsorbed oxygen on gold and dissociatively adsorbed hydrogen [50]. Thus, the band at 3500–3200 cm^{-1} observed on the $Au/CeO_2–Co_3O_4$ catalyst may also be ascribed to the –OOH species. As soon as the catalyst comes in contact with the PROX mixture ($CO/O_2/H_2$ atmosphere), surface gold species are covered with these –OOH species. Generation of hydroperoxy intermediates from synergy between H_2 and O_2 would be driven by the formation of O–H bonds that enhance O–Au interactions [51]. Actually, these highly oxidative intermediates in different systems have been identified by means of high-resolution scanning tunneling microscopy (STM) [52], inelastic neutron scattering [53], and UV–vis/X-ray absorption spectroscopy [54]. Moreover, several other studies on the promotional effect of hydrogen or water have shown the ability of water-related species to oxidize CO [46,48]. In the absence of CO or propylene, these species would be readily converted to water via OH intermediates [50].

The possible reaction mechanism involving hydroperoxy intermediates is proposed. The CO PROX over $Au/CeO_2–Co_3O_4$ catalyst may proceed via the reaction of Au-bonded CO with hydroperoxy (OOH) intermediates. Firstly, the Au undergoes oxidation to form an effective "Au-oxide" ($Au^{\delta+}$) species as confirmed by XPS, and H_2 dissociatively adsorbed on gold recombines with the atomic oxygen in the Au-oxide to form –OOH and/or –OH species. CO adsorbed on metallic Au sites then reacts with the highly active –OOH intermediate to form CO_2, and simultaneously leaves behind a hydrogen atom (H^*) and an oxygen vacancy in the Au-oxide. Next, an O_2 molecule is adsorbed and activated on the oxygen vacancy, which subsequently reacts with the remaining H^* to form new –OOH species and gets the CO oxidation running.

On the other side, the pathway through the conversion and decomposition of carbonate-like species to CO_2 induced by water cannot be excluded from the reaction mechanism. In comparison with the CO/H_2 adsorption over $Au/CeO_2–Co_3O_4$ catalyst, the peaks related to surface carbonates disappear in $CO/H_2/O_2$ co-adsorption. The reasons maybe that (1) the reoxidization of the reduced centers by the oxygen in the stream suppresses the formation of carbonate species; (2) the formation of water through the reaction of hydrogen with oxygen under the PROX condition induces the conversion and decomposition of carbonate species [55].

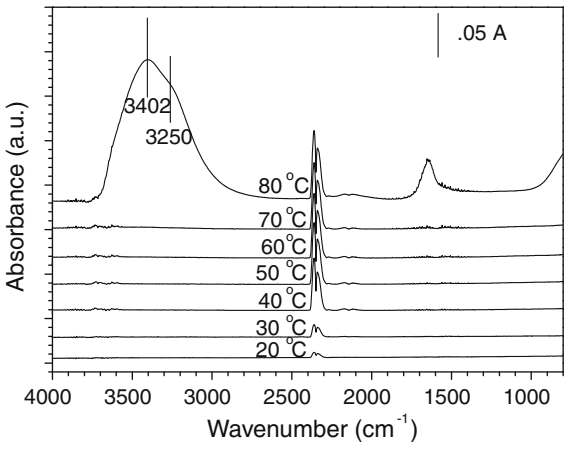

Fig. 10. DRIFTS spectra of $CO/H_2/O_2$ co-adsorption in (1% CO + 1% O_2 + 50% H_2)/Ar flow on the $Au/CeO_2–Co_3O_4$ catalyst at different temperatures.

3.7.4. Origins of the deactivation on the $Au/CeO_2–Co_3O_4$ catalyst

The HRTEM images and XRD patterns of the $Au/CeO_2–Co_3O_4$ catalysts show that the Au particles are not obviously aggregated or sintered. Thus, sintering of the Au particles can be excluded from the origins of deactivation.

The deactivation of the catalyst is due to an intrinsic transformation in the catalytic properties of $Au/CeO_2–Co_3O_4$, including the change in the chemical state of gold species ($Au^{\delta+}$ or Au^0) and the support oxides. The XPS study reveals that both Au^0 and $Au^{\delta+}$ species are present in the fresh catalyst. The result supports the hypothesis suggested by Bond and Thompson that both Au^0 and $Au^{\delta+}$ are essential for CO PROX [16]. These two species play important roles for the CO adsorption and the –OOH formation, respectively. Meanwhile, the experiment demonstrates a reduction of the active $Au^{\delta+}$ species in the deactivated catalyst. The disappearance of $Au^{\delta+}$ may indicate that the interaction between gold and support is weakened. Therefore, it is deduced that the reduction of $Au^{\delta+}$ may be the origin of the high deactivation rate on the $Au/CeO_2–Co_3O_4$ catalyst during the first 100 h in the CO PROX reaction process as shown in Fig. 1.

The reduction of the support oxides surrounding the gold particles in the reducing operating conditions is also confirmed to be an origin for the deactivation of the $Au/CeO_2–Co_3O_4$ catalyst in CO PROX. The HRTEM, XRD, XPS, and H_2-TPR studies demonstrate that Co_3O_4 is reduced to CoO, the interaction between CeO_2 and Co_3O_4 is destroyed, and the defects sites for oxygen activation decrease very much. All these may suppress the supplement of active oxygen and the formation of –OOH species, inhibit the CO oxidation reaction, and lead to the deactivation of the catalyst.

The deactivation of the $Au/CeO_2–Co_3O_4$ catalyst is also attributed to the formation of carbonates and H_2O in the CO PROX process via the blockage of the active sites as confirmed by DRIFTS and O_2-TPO. Moreover, the DRIFTS spectra clearly show that intense H_2O and a marginal increase in the amount of carbonate species are present in the $CO/H_2/O_2$ co-adsorption on the $Au/CeO_2–Co_3O_4$ catalyst, while only carbonate-like species are detected in the CO adsorption and CO/H_2 co-adsorption. The phenomena indicate that hydration of the catalyst surface, which is closely related with the presence of oxygen in the reaction gas, might play a great or even greater role than the formation of carbonate-like species in the deactivation of the catalyst. Furthermore, the water produced via the H_2 oxidation will condense inside the pores, and therefore CO and H_2 concentrations at the catalytic sites will be massively influenced by the mass transfer phenomena. Although the formation of carbonate and H_2O is continuous in the PROX reaction process, the effect becomes fatal in the final period of the catalyst deactivation due to the full blockage of the active sites, which directly causes a decrease in the conversion of both O_2 and CO. Thus, the blockage of the catalytic sites by carbonates and condensing H_2O combined with the hydration of the catalyst surface (the latter may be more important) may be responsible for the complete deactivation of $Au/CeO_2–Co_3O_4$ catalyst during the last 40 h in the CO PROX reaction process as shown in Fig. 1.

Anyway, the deactivation is reversible. When the deactivated $Au/CeO_2–Co_3O_4$ catalyst is calcined in a flowing air at 200 °C, its initial activity is almost fully regenerated. The release of CO_2 and water detected in the regeneration process provides evidence that the hydration of the catalyst surface and the accumulation of carbonates are the origins of the deactivation.

4. Conclusions

The origins of the deactivation of a $Au/CeO_2–Co_3O_4$ catalyst during CO PROX are investigated in detail by HRTEM, XRD, XPS, H_2-TPR, O_2-TPO, and DRIFTS. A possible mechanism involving –OOH inter-

mediate is suggested and used to explain the deactivation process. The deactivation of the catalyst is mainly due to an intrinsic transformation in the chemical state of gold species and the support oxides in the $Au/CeO_2–Co_3O_4$ catalyst. The reduction of $Au^{\delta+}$ to Au^0 and of Co_3O_4 to CoO, accompanied with a structure reordering, suppresses the supplement of active oxygen and the formation of –OOH species, inhibits the CO oxidation reaction, and leads to the deactivation of the catalyst. The blockage of the active sites by carbonates and H_2O formed during the reaction process is responsible for the complete deactivation of the catalyst, and the hydration of the catalyst surface may play a more important role than the formation of carbonate-like species in the deactivation of the catalyst.

Acknowledgments

The authors are grateful for the financial support of the State Key Fundamental Research Project and the Natural Science Foundation of China (20773155) and Shanxi Province (2007011037).

References

[1] A.S.K. Hashmi, G.J. Hutchings, Angew. Chem. Int. Ed. 45 (2006) 7896.
[2] D. Teschner, A. Wootsch, O. Pozdnyakova-Tellinger, J. Kröhnert, E.M. Vass, M. Hävecker, S. Zafeiratos, P. Schnörch, P.C. Jentoft, A. Knop-Gericke, R. Schlögl, J. Catal. 249 (2007) 318.
[3] Y. Huang, A. Wang, X. Wang, T. Zhang, Int. J. Hydrogen Energ. 32 (2007) 3880.
[4] M. Kuriyama, H. Tanaka, S. Ito, T. Kubota, T. Miyao, S. Naito, K. Tomishige, K. Kunimori, J. Catal. 252 (2007) 39.
[5] D. Gamarra, A. Hornés, Z. Koppány, Z. Schay, G. Munuera, J. Soria, A. Martínez-Arias, J. Power Sources 169 (2007) 110.
[6] P. Landon, J. Ferguson, .B.E. Solsona, T. Garcia, A.F. Carley, A.A. Herzing, C.J. Kiely, S.E. Golunski, G.J. Hutchings, Chem. Commun. (2005) 3385.
[7] G. Avgouropoulos, T. Ioannides, Ch. Papadopoulou, J. Batista, S. Hocevar, H.K. Matralis, Catal. Today 75 (2002) 157.
[8] A.M.D. de Farias, A.P.M.G. Barandas, R.F. Perez, M.A. Fraga, J. Power Sources 165 (2007) 854.
[9] C.K. Costello, M.C. Kung, H.S. Oh, Y. Wang, H.H. Kung, Appl. Catal. A 232 (2002) 159.
[10] S.S. Pansare, A. Sirijaruphan, J.G. Goodwin jr., J. Catal. 234 (2005) 51.
[11] L.H. Chang, N. Sasirekha, Y.W. Chen, Catal. Commun. 8 (2007) 1702.
[12] W. Deng, J.D. Jesus, H. Saltsburg, M. Flytzani-Stephanopoulos, Appl. Catal. A 291 (2005) 126.
[13] G.C. Bond, C. Louis, D.T. Thompson, Catalysis by Gold, Imperial College Press, London, 2006. p. 12.
[14] Z. Ma, S. Brown, S.H. Overbury, S. Dai, Appl. Catal. A 327 (2007) 226.
[15] T.V. Choudhary, D.W. Goodman, Top. Catal. 21 (2002) 25.
[16] G. C Bond, D. T Thompson, Gold Bull. 33 (2000) 41.
[17] G.J. Hutchings, M.S. Hall, A.F. Carley, P. Landon, B.E. Solsona, C.J. Kiely, A. Herzing, M. Makkee, J.A. Moulijn, A. Overweg, J.C. Fierro-Gonzalez, J. Guzman, B.C. Gates, J. Catal. 242 (2006) 71.
[18] J.C. Fierro-Gonzalez, J. Guzman, B.C. Gates, Top. Catal. 44 (2007) 103.
[19] J. Steyn, G. Pattrick, M.S. Scurrell, D. Hildebrandt, M.C. Raphulu, E. van der Lingen, Catal. Today 122 (2007) 254.
[20] M. Haruta, Gold Bull. 37 (2004) 27.
[21] P. Konova, A. Naydenov, Cv. Venkov, D. Mehandjiev, D. Andreeva, T. Tabakova, J. Mol. Catal. A: Chem. 213 (2004) 235.
[22] R. Zanella, C. Louis, Catal. Today 107–108 (2005) 768.
[23] B. Schumacher, V. Plzak, M. Kinne, R.J. Behm, Catal. Lett. 89 (2003) 109.
[24] C.H. Kim, L.T. Thompson, J. Catal. 230 (2005) 66.
[25] R. Burch, Phys. Chem. Chem. Phys. 8 (2006) 5483.
[26] M. Haruta, Catal. Today 36 (1997) 153.
[27] H. Wang, H.Q. Zhu, Z.F. Qin, G.F. Wang, F.X. Liang, J.G. Wang, Catal. Commun. 9 (2008) 1487.
[28] H.Q. Zhu, Z.F. Qin, W.J. Shan, W.J. Shen, J.G. Wang, J. Catal. 225 (2004) 267.
[29] L.F. Liotta, G. Di Carlo, G. Pantaleo, A.M. Venezia, G. Deganello, Appl. Catal. B 66 (2006) 217.
[30] D.A. Bulushev, I. Yuranov, E.I. Suvorova, P.A. Buffat, L. Kiwi-Minsker, J. Catal. 224 (2004) 8.
[31] M. Manzoli, F. Boccuzzi, A. Chiorino, F. Vindigni, W. Deng, M. Flytzani-Stephanopoulos, J. Catal. 245 (2007) 308.
[32] E. Bêche, P. Charvin, D. Perarnau, S. Abanades, G. Flamant, Surf. Interface Anal. 40 (2008) 264.
[33] M.M. Natile, A. Glisenti, Chem. Mater. 17 (2005) 3403.
[34] M. Kang, M.W. Song, C.H. Lee, Appl. Catal. A 251 (2003) 143.
[35] J. Guzman, B.C. Gates, J. Am. Chem. Soc. 126 (2004) 2672.
[36] Z. Liu, S.J. Jenkins, D.A. King, Phys. Rev. Lett. 94 (2005) 196102.
[37] J.-Y. Luo, M. Meng, X. Li, X.-G. Li, Y.-Q. Zha, T.-D. Hu, Y.-N. Xie, J. Zhang, J. Catal. 254 (2008) 310.
[38] K. Ichimura, Y. Inoue, I. Yasumori, Bull. Chem. Soc. Jpn. 53 (1980) 3044.
[39] Q. Guo, Y. Liu, Appl. Catal. B 82 (2008) 19.
[40] M. Hoang, A.E. Hughes, T.W. Turney, Appl. Surf. Sci. 72 (1993) 55.
[41] J. Jansson, J. Catal. 194 (2000) 55.
[42] Y.A. Lokhov, S.F. Tikhov, M.N. Bredikhin, A.G. Zhirnyagin, V.A. Sadykov, Mendeleev Commun. 2 (1992) 10.
[43] G. Avgouropoulos, M. Manzoli, F. Boccuzzi, T. Tabakova, J. Papavasiliou, T. Ioannides, V. Idakiev, J. Catal. 256 (2008) 237.
[44] A.M. Garrido Pedrosa, M.J.B. Souza, D.M.A. Melo, A.S. Araujo, L.B. Zinner, J.D.G. Fernandes, A.E. Martinelli, Solid State Sci. 5 (2003) 725.
[45] E. Quinet, F. Morfin, F. Diehl, P. Avenier, V. Caps, J.-L. Rousset, Appl. Catal. B 80 (2008) 195.
[46] T.S. Kim, J. Gong, R.A. Ojifinni, J.M. White, C.B. Mullins, J. Am. Chem. Soc. 128 (2006) 6282.
[47] M. Daté, M. Haruta, J. Catal. 201 (2001) 221.
[48] L. Piccolo, H. Daly, A. Valcarcel, F.C. Meunier, Appl. Catal. B 86 (2009) 190.
[49] E. Quinet, L. Piccolo, H. Daly, F.C. Meunier, F. Morfin, A. Valcarcel, F. Diehl, P. Avenier, V. Caps, J.L. Rousset, Catal. Today 138 (2008) 43.
[50] D.G. Barton, S.G. Podkolzin, J. Phys. Chem. B 109 (2005) 2262.
[51] L. Barrio, P. Liu, J.A. Rodriguez, J.M. Campos-Martin, J.L.G. Fierro, J. Phys. Chem. C 111 (2007) 19001.
[52] J. Matthiesen, S. Wendt, J. Hansen, G.K.H. Madsen, E. Lira, P. Galliker, E.K. Vestergaard, R. Schaub, E. Lægsgaard, B. Hammer, F. Besenbacher, ACS Nano 3 (2009) 517.
[53] C. Sivadinarayana, T.V. Choudhary, L.L. Daemen, J. Eckert, D.W. Goodman, J. Am. Chem. Soc. 126 (2004) 38.
[54] J.J. Bravo-Surez, K.K. Bando, J. Lu, M. Haruta, T. Fujitani, T. Oyama, J. Phys. Chem. C 112 (2008) 1115.
[55] B. Schumacher, Y. Denkwitz, V. Plzak, M. Kinne, R.J. Behm, J. Catal. 224 (2004) 449.